Cyclic Behavior of Multi-Row Slit Shear Walls Made from Low Yield Point Steel

AUTHOR(S):

He, Liusheng; Togo, Takuma; Hayashi, Kazuhiro; Kurata, Masahiro; Nakashima, Masayoshi

CITATION:

He, Liusheng ...[et al]. Cyclic Behavior of Multi-Row Slit Shear Walls Made from Low Yield Point Steel. Journal of Structural Engineering 2016, 142(11): 9: 04016094.

ISSUE DATE:

2016-11

URL:

http://hdl.handle.net/2433/264026

Cyclic Behavior of Multi-Row Slit Shear Walls Made from Low Yield Point Steel

Liusheng He[1]; Takuma Togo[2]; Kazuhiro Hayashi[3]; Masahiro Kurata, M.ASCE[4]; and Masayoshi Nakashima, M.ASCE[5]

Abstract: The steel slit shear wall has attracted much attention as a lateral force-resisting system. However, issues, such as fractures formed at the slit ends and pinched hysteresis, reduce energy dissipation. To address these issues, the authors have developed a steel slit shear wall made from low yield point steel that has a low yield stress and large ductility and strain hardening. Steel slit shear walls made from low yield point steel dissipated energy at small lateral drifts, shear deformation was evenly distributed among all rows, fracture was eliminated, and "fat" hysteresis without the requirement for out-of-plane constraints was feasible. By adjusting dimensions of the link (segment divided by slits) and the number of rows of links while maintaining the required shear strength and stiffness, a small width-to-thickness ratio for the links was achievable to ensure the in-plane behavior of links and thus good energy dissipation. The combined hardening model in ABAQUS simulated well the large strain hardening of low yield point steel. A proposed design procedure that ensures good energy dissipation was given.

Author Keywords: Steel slit shear wall; Low yield point steel; Strain hardening; Width-to-thickness ratio; Cyclic tests.

Introduction

Shear wall systems that use steel plates are common in earthquake engineering because of their large stiffness, lightness, and ductility. Among the many types of steel shear walls, the steel plate shear wall (SPSW) and steel slit shear wall (SSSW) are common in Japanese seismic

[1]Research Fellow, Disaster Prevention Research Institute, Kyoto Univ., Gokasho, Uji, Kyoto, Japan (corresponding author). Email: liush.he@gmail.com
[2]M.S. Candidate, Dept. of Arch. and Arch. Sys., Grad. Sch. of Eng., Kyoto Univ., Kyodai-Katsura, Kyoto, Japan.
[3]Assistant Professor, Dept. of Arch. and Civil Eng., Toyohashi Univ. of Technology, Toyohashi, Japan.
[4]Associate Professor, Disaster Prevention Research Institute, Kyoto Univ., Gokasho, Uji, Kyoto, Japan.
[5]Professor, Disaster Prevention Research Institute, Kyoto Univ., Gokasho, Uji, Kyoto, Japan.

design. The SPSW is accepted extensively in North America and is included in design standards [e.g., AISC 2010; CSA 2009]. It resists shear deformation with tension field action after the onset of buckling and presents substantial pinching behavior in its hysteresis loop [e.g., Roberts and Ghomi (1991); Vian (2005); Berman and Bruneau (2005); Qu et al. (2008)]. The concept of an SSSW is illustrated in Fig. 1. This wall is fabricated from steel plate and has a series of rectangular segments (termed links) that are formed by laser-cutting vertical slits. When the wall undergoes in-plane shear deformation (referred to as lateral drift), each link behaves as a flexural member at the point of inflection located at mid-height. The yielding and hysteresis of links become a source of energy dissipation similar to conventional steel hysteresis dampers (Martinez-Rueda 2002). Since Hitaka and Matsui (2003) introduced the design philosophy of SSSWs, many studies, including practical applications to real buildings, have been reported on [e.g., Hitaka et al. (2007, 2009); Cortes and Liu (2011); Ke and Chen (2012)].

Energy dissipation of an SSSW is controlled by the link's width-to-thickness ratio (b/t) and aspect ratio (l/b). Wider links (large b/t) can yield a greater strength and stiffness. However, if the link is too wide in comparison with its thickness, local buckling of the link occurs and this decreases the energy dissipation. Different means have been proposed to prevent link buckling [e.g., Hitaka et al. (2009); Ma et al. (2010); Cortes and Liu (2011)]. However, improvements in energy dissipation were mediocre and adverse effects resulted. Because links cannot buckle out of plane to distribute the deformation with the buckling restraint, stress concentrations at the ends of the link accelerate fracture formation, which may result in brittle failure. If the link is too long (large l/b), it becomes too flexible and its energy dissipation is decreased significantly. For relatively short links, the arrangement of links in multiple rows (m) can be used. However, concentrated fracture on a single row may occur, as observed in the work of Cortes and Liu

(2011). Further investigation is required to eliminate fractures at the ends of the link, and especially their concentration in a single row.

Low yield point steel (LYP), which has a low initial yield stress, large ductility, and exhibits strain hardening, is a possible practical solution. SSSWs made from LYP enter the plastic stage more rapidly than their surrounding frame. The large strain hardening of LYP enables plasticity expansion over larger regions and thus dissipates more energy, and the large ductility of LYP eliminates fracture at the ends of the link. When equal lateral bearing capacity is expected, SSSWs made from LYP must be thicker relative to those made from conventional steel. The increased thickness delays local buckling of individual links and thus there is a reduced need for out-of-plane constraints. The application of LYP to shear walls is not new, and has been presented in the work of Nakashima et al. (1995), Matteis et al. (2003), Chen and Jhang (2006), and Zhang et al. (2012), but no work has been conducted on the application of such steel to slit shear walls.

The authors propose an unstiffened SSSW design using LYP for improved energy dissipation. Quasi-static cyclic testing on four 1/3-scaled SSSW specimens was conducted. A series of comparative investigations were used to assess the performance of SSSWs made from LYP and prediction of shear strength, stiffness, and hysteretic behavior.

Strength and stiffness

An SSSW must have sufficient strength to resist the lateral load and sufficient stiffness to satisfy the design criterion on lateral drift. For an individual link, using the classical beam theory, the shear force that corresponds to the first yielding at the ends of the link, termed the yield strength $Q_{y.link}$, is:

$$Q_{y.link} = \frac{2M_y}{l} = \frac{b^2 t}{3l}\sigma_y , \tag{1}$$

where $M_y = b^2 t / 6\sigma_y$ is the moment at the end of the link when first yielding begins, b is the width of the link, l is the length of the link, t is the plate thickness, and σ_y is the yield stress.

Assuming that the plastic hinge is formed at the ends of the link where maximum strain occurs, the shear force that corresponds to full plasticity, termed the plastic strength $Q_{P.link}$, is:

$$Q_{P.link} = 1.5 Q_{y.link} \tag{2}$$

For an SSSW with links in multiple rows (Fig. 1), the total yield/plastic strength is estimated by summation of all individual links:

$$Q_y = \sum_{i=1}^{n} \frac{tb^2}{3l}\sigma_y = \frac{ntb^2}{3l}\sigma_y = \frac{Bt}{3\alpha}\sigma_y, \tag{3}$$

$$Q_p = 1.5 Q_y, \tag{4}$$

where $B = bn$ is the width of the wall neglecting the width of slits and $\alpha = l / b$ is the aspect ratio of the link.

The elastic stiffness of the SSSW was proposed by Hitaka and Matsui (2003), and is calculated by summing all contributions from individual links and unslitted portions, as given in Eq. (5). Shear and flexural deformations of individual links are considered, and the contribution of an unslitted portion is accounted for through its shear deformation.

$$K = \frac{1}{\dfrac{1.2(H-ml)}{GBt} + \gamma \dfrac{l^3}{Etb^3}\dfrac{m}{n} + \dfrac{1.2l}{Gbt}\dfrac{m}{n}} = \frac{Bt / H}{\dfrac{1.2}{G} + \gamma \dfrac{\beta\alpha^2}{E}}, \tag{5}$$

where E is Young's modulus; G is the shear modulus; 1.2 is the shear deformation shape factor for a rectangular section; $\gamma = (1 + 1/\alpha)^3$ is a multiplier that reflects the flexibility at the ends of the flexural links, with $\gamma = 1$ denoting a perfectly rigid boundary and otherwise $\gamma > 1$; m is the number of rows of links; n is the number of links in one row; H is the height of the wall; and $\beta = ml / H$ is the slit fraction, which is the ratio of total link length to wall height.

A noteworthy feature of the SSSW is that the shear strength and stiffness can be designed separately. Given the overall dimensions and material properties of the wall, the yield strength is dependent solely on the link's aspect ratio (α) (Eq. (3)) and the stiffness is determined from α and the slit fraction (β) (Eq. (5)), regardless of n and m. Therefore, the same values of α and β guarantee the same yield strength and stiffness without a need to change the overall dimensions and material properties of the wall, which provides flexibility in the design.

Test preparation

Material properties

Mild steel SS400, which is commonly used in Japan and has a specified minimum ultimate strength of 400 MPa, and LYP100, which is an LYP with a nominal yield stress of 100 MPa, were used. Compared with SS400, LYP100 has a lower initial yield stress and larger ductility and strain hardening. These properties allow for early material yielding starting from a small lateral drift and ensure good deformation capacity. Based on uniaxial tensile tests, SS400 has a yield stress of 304 MPa and an ultimate stress of 431 MPa; LYP100 has a yield stress of 96 MPa and an ultimate stress of 269 MPa. Fig. 2 shows the obtained stress-strain relationships.

A cyclic loading test of an SSSW made from LYP100, with four 90-mm-wide links (overall dimensions of 360 mm × 360 mm) using a 9-mm-thick plate (Fig. 3(a)), was used to calibrate the material properties of LYP100 for numerical simulation. The solid lines of Fig. 3(b) show the hysteretic curves obtained from the test.

In the numerical simulation, the commercial finite element code ABAQUS 6.10 (Dassault Systèmes, 2004) was used, in which a three-dimensional four-node shell element with reduced integration was used to represent the plate. The combined hardening model in ABAQUS was used to model both the kinematic and isotropic hardening of LYP100. The kinematic hardening property was determined from the results of the tensile coupon test. For the isotropic hardening, a phenomenological curve fitting process was conducted, in which the input parameters were adjusted until a reasonable match over most of the loading history was obtained. The numerical results are plotted using dashed lines in Fig. 3(b). The numerical simulation was able to capture the hysteretic behavior with reasonable accuracy.

Test specimen

The prototype building where the SSSWs are installed is a medium-rise steel frame building with a story height of 3500 mm and a span length of 5600 mm. The shear wall is proposed to occupy the entire span with a yield strength of 800 kN. This strength is equivalent to a pair of braces using a square hollow structural section of 175 mm × 175 mm × 6 mm made from A36 steel and placed in a chevron arrangement. Four 1/3-scaled SSSW specimens are designed with overall specimen dimensions of 1150 mm × 1840 mm.

For a typical frame of a weak-beam strong-column type, a story drift of 0.5% is assumed to be the elastic limit. Scaled-down specimens were designed to enter plasticity earlier than the frame. Specimens 1–3, made from LYP100 with a plate thickness of 9 mm, were designed to yield at 1/4 the elastic limit of the frame. Specimen 4, made from SS400 with a plate thickness of 4.2 mm, was designed to yield later at half the elastic limit of the frame. Link dimensions and the number of rows of links in Specimens 1–3 (with links in two, three, and six rows, respectively) were adjusted such that they had the same yield strength Q_y of 89 kN (estimated using Eq. (3)) and elastic stiffness K of 70 kN/mm (estimated using Eq. (5)). Specimen 4 with links in two rows had a Q_y of 103 kN and a K of 36 kN/mm. The slightly smaller yield strengths of Specimens 1–

3 than Specimen 4 were designed with the consideration of a larger strain hardening of LYP100. Four specimens have the same shear strength at a drift ratio of 1%, which will be presented in the discussion of the test results. Table 1 summarizes the major parameters of each specimen.

Fig. 4 shows details of the four specimens. Vertical slits were made by a digitally controlled laser cutting machine. Each specimen had top and bottom portions with round holes for connection to the loading frame. The top and bottom portions were 90 mm and 100 mm deep, respectively. Double-sided angles and high-strength bolts were used.

Test setup, instrumentation, and loading protocol

The test setup was a portal frame with four pins at each corner, a height of 1748 mm, and a column centerline spacing of 3000 mm, as shown in Fig. 5. The lateral deformation of the test setup was controlled automatically using the loading system, which consists of a horizontal hydraulic jack, a hydraulic pump system, and a control computer. The main components of the test bed were: (a) top and bottom H-400 × 400 × 13 × 21 beams, (b) two H-250 × 250 × 9 × 16 columns, (c) four pin subassemblies, and (d) a fixed support for the actuator loading. The deformation of the test setup was restrained to remain in plane using out-of-plane restrainers and guiding beams.

The lateral drift applied to the shear wall was controlled by the jack's displacement. The net shear deformation into the links was measured by attaching two displacement transducers at the ends of the link in certain rows, as shown in Fig. 5(c). For Specimens 1, 2, and 4, the net shear deformation into the links in all rows was measured. For Specimen 3 with six rows, the net shear deformation of links was measured in the second, fourth, and sixth row from the top. Out-of-plane deformation at the vertical center of the wall edge (D5 in Fig. 5(c)) was measured to detect the onset of plate buckling.

The incremental two-cycle loading, which was adopted often in the experimental study of shear walls, was used as shown in Fig. 6. At lateral drifts smaller than a drift ratio of 2%, the incremental amplitude was a drift ratio of 0.25%. At lateral drifts larger than a drift ratio of 2%, the incremental amplitude was a drift ratio of 0.5%. The same amplitudes were repeated twice to a maximum drift ratio of 4%.

Discussion of test results

Yield strength

Yielding and plastification developed at the ends of the link is a unique feature of the SSSW system. To observe the first yielding, foil strain gauges for measuring the elastic strains were glued on the center links in each row, and on the front face of the links at their ends, as shown in Fig. 5(c). The gauges were glued in the longitudinal direction of the link and 3 mm inside its edge (Fig. 5(d)).

The yield strength was determined as the shear force applied to the specimen when one of the strain gauges exceeded the yield strain obtained from the coupon test. The yield strengths obtained are listed in Table 2, together with the analytical strength estimated using Eq. 3. The experimental and analytical strengths were similar, with an error of 16% for Specimens 3 and errors less than 6% for the others.

As mentioned previously, four specimens were designed to have the same shear strength at a drift ratio of 1%. The strengths at a drift ratio of 1%, $Q_{1\%.t}$, are listed in Table 2 and were similar for all specimens, with a variance within 4%.

Maximum strength

The maximum strength obtained from the test is listed in Table 2. Here, the maximum strength $Q_{\max.t}$ was defined as the largest absolute strength obtained to completion of the loading with a drift ratio of 4%. The maximum strength was 25% larger than the plastic strength Q_p (estimated using Eq. 4) for Specimen 4 made from SS400. For Specimens 1–3 made from LYP100, the maximum strength was 2.1–2.4 times Q_p. The significant overstrength relative to Q_p, especially for SSSWs made from LYP100, is ascribed to the combined effects of strain hardening and tension fields formed at large drift ratios, which will be explained more in a later section. To estimate the maximum strength in the design of beams and connecting angles where the SSSW is installed, an amplification of the plastic strength should be considered cautiously. For SSSWs made from LYP100 with a maximum drift ratio of 4%, 2.5 times Q_p can be used in the estimation of maximum strength.

Initial stiffness

The initial stiffness obtained from the test is also listed in Table 2. The predicted elastic stiffness (K) agreed relatively well with the test results (K_t), with an error of less than 2%. Specimen 4 made from SS400 entered into plasticity at a drift ratio of approximately twice that of Specimens 1–3 made from LYP100 as designed. The yielding sequence, yielding of the slit wall prior to the frame, was well controlled. The very similar stiffness (and shear strength) of Specimens 1–3, with different link dimensions and number of rows of links, demonstrated the flexibility in the SSSW design.

Shear deformation distribution among link rows

The net shear deformation into links was measured by the relative displacement between the two ends of the link in the same row. Taking Specimen 1 in Fig. 5(c) as an example, the difference between D1 and D2 gives the net shear deformation for the links in the first row and the difference between D3 and D4 gives the net shear deformation for the links in the second row. Fig. 7 shows the shear deformation distribution among rows. Within a story drift ratio of 1%, the net shear deformation for the links in Specimens 1–3 made from LYP100 was almost the same among all rows. For Specimen 4 made from SS400 (Fig. 7(a)), the net shear deformation measured on the first row was larger. This difference is caused primarily by the different nature of the two grades of steel. Under in-plane shear deformation, the initial imperfection in the plate, including geometrical imperfections such as non-uniform thickness or material defects such as cracks and vacancies, triggered a slightly different allocation of shear deformation among the rows. The large strain hardening of the LYP100 allowed the stress to increase with the development of plasticity, which adaptively adjusted the shear strength of each row and prevented the formation of a weak row with larger deformation. On the contrary, because of the limited strain hardening of SS400 used in Specimen 4, the increase in stress at the row that experienced a larger deformation was insufficient to transform it into a stronger row and thus the uneven deformation was maintained.

Local buckling and fracture of individual links

In the thin plate theory, the width-to-thickness ratio controls local buckling (Timoshenko and Gere, 1961). For individual links with a suitable link height, the width-to-thickness ratio of the link (b/t) controls the inelastic behavior. The early local buckling of links with a large b/t reduces the energy dissipation. To ensure the in-plane behavior of links, a small enough b/t is needed, which can be realized by cutting more slits into the wall and accordingly having more narrow links (n). To maintain the same shear strength and stiffness, shorter links should be arranged in more rows (m). Taking Specimens 1–3 made from LYP100 for example, the same aspect ratio of the link ($\alpha = l / b$ of 5.9) and slit fraction ($\beta = ml / H$ of 0.7) provided the same strength and stiffness, whereas the values of b/t are 7.8, 5.1, and 2.5, with links arranged in two, three, and six rows, respectively. Notable local buckling of links in Specimen 1 occurred at a drift ratio of 3.5%, but this behavior was not observed in Specimens 2–3 because of their smaller values of *b*/*t*. With the steel of LYP100 used in this study, a *b*/*t* of 5.1 in Specimen 2 is considered small enough to ensure the in-plane behavior of links. With a *b*/*t* of 7.8, which is the same as that of Specimen 1, Specimen 4 made from SS400 exhibited local buckling of links at an earlier drift ratio of 2%, together with the initiation of fracture at the ends of the link because of the reduced ductility of SS400. Because Specimens 1 and 4 had approximately the same shear strengths, the greater thickness of Specimen 1 (9 mm, and 4.2 mm for Specimen 4) resulted in a low stress level, which explained the delayed local buckling of links in Specimen 1.

Fig. 8 shows the deformed specimens. Of Specimens 1–3 made from LYP100, only Specimen 1 exhibited notable local buckling of links and no sign of fracture throughout the loading in all specimens. For Specimen 4 made from SS400, local buckling and fracture at the ends of the link occurred simultaneously at a drift ratio of 2% and finally penetrated a majority of links in the second row after completion of the first cycle of a drift ratio of 3.2%.

Effect of slit fraction

In the direction of the wall's height, the proportion of individual links, represented by the slit fraction $\beta = ml / H$, is also an important factor. A small β indicates short individual links and a large unslitted portion. Because of the height difference of the link and the wall, short links have a high strain level at the ends of the link subjected to the same lateral drift, which would cause early local buckling of links. The behavior of the wall is dominated more by the plate rather than by the individual links because of a large unslitted portion.

As shown in Fig. 5(c), the out-of-plane deformation at the wall edge (D5) was measured by a displacement transducer to detect the onset of plate buckling. Specimens 1–3, with a β of 0.7, showed a similar out-of-plane deformation. For illustration, only Specimen 1 is discussed here.

The out-of-plane deformation of Specimen 1 was observed at a drift ratio of 1%, with a normalized deformation of 1/280 (defined as the absolute out-of-plane displacement divided by the wall height). For Specimen 4, with a β of 0.42, the out-of-plane deformation occurred at a drift ratio of 0.25%, with a normalized out-of-plane deformation of 1/300. This much earlier onset of out-of-plane deformation of Specimen 4 was believed to result from the small β of 0.42, which promoted the overall plate behavior more significantly than the behavior of individual links. With the increase in drift ratios, the out-of-plane deformation of all specimens increased. At a drift ratio of 1%, the normalized out-of-plane deformation of Specimen 4 was 1/110 and remained approximately constant for further loading. The concentration of deformation in a lower link was a likely source for this behavior. Specimen 1 sustained a steadily increasing out-of-deformation for larger drifts, but the normalized out-of-plane deformation remained 1/35 at a drift ratio of 2%. (After 2%, the displacement transducer was removed to prevent it from being damaged in case the deformation were beyond its range.) Considering that the middle part of the wall had a much smaller out-of-plane deformation than the wall edge and no deterioration of the shear strength appeared in the overall hysteretic behavior, the effect of out-of-plane deformation was considered at most secondary.

Conversely, a large β yields a short unslitted portion between the rows of links. Yielding that developed at the ends of the link is likely to expand over this portion, and if the unslitted portion is too short, the assumption of a stiff boundary between the links will no longer be valid, which also limits further development of plasticity at the ends of the link and thus lessens the energy dissipation. The value of β is recommended as 0.65–0.85 by McCloskey (2006) to ensure that the wall behavior is controlled by the links. A β of 0.7 for Specimens 1–3 follows this recommendation.

Energy dissipation behavior

The solid lines of Fig. 9 show the hysteretic curves, with the ordinate being the shear force normalized by the plastic strength (Q_p). Within a drift ratio of 1%, the effect of large strain hardening of LYP100 was demonstrated clearly by the isotropic "fatness" of the hysteretic loops. Beyond a drift ratio of 1%, the strength increment slowed down but continued to grow with the increase in lateral drift because of the formation of tension fields. Local buckling of links in Specimen 1 caused slight pinching in the hysteresis starting from a drift ratio of 3.5%. Local buckling of links did not occur in Specimens 2–3 and "fat" hysteretic loops resulted. For Specimen 4 made from SS400, the shear strength degraded significantly after fracture occurred at the ends of the link at a drift ratio of 2%. By using the steel of LYP100 with large strain hardening, an out-of-plane constraint is not required to obtain "fat" hysteretic loops.

The equivalent damping ratios estimated using the standard procedure (Chopra, 2000) are plotted for each drift ratio in Fig. 10, in which one loop in the first cycle was used for the calculation. The equivalent damping ratios of Specimens 1–3 made from LYP100 was approximately two times that of Specimen 4 made from SS400 before a drift ratio of 1%. Beyond a drift ratio of 1%, the equivalent damping ratios of Specimens 1–3 were almost constant with a ratio of 0.4 until completion of loading with a drift ratio of 4%.

Fig. 11 shows the energy dissipation, estimated as the summation of energy dissipated in the first cycle at each drift ratio. Specimens 1–3 made from LYP100 dissipated nearly the same energy to a drift ratio of 3.5%. At a drift ratio of 0.25%, the energy dissipation of Specimens 1–3 was 6.6 times that of Specimen 4, until the completion of loading of Specimen 4 at a drift ratio of 3.2%. The energy dissipation of Specimens 1–3 was no less than 1.7 times that of Specimen 4. After 3.5% with further local buckling of links of Specimen 1, the energy dissipated decreased by 13% at a drift ratio of 4%, compared with Specimens 2–3 where local buckling of individual links did not occur.

Numerical analysis

The hysteretic curves in dashed lines in Fig. 9 show the numerical results obtained from ABAQUS. For Specimens 1–3 made from LYP100, the material properties calibrated in advance (Fig. 3) were adopted and the simulation predicted relatively well the maximum strength and hysteretic curve. For Specimen 4 made from SS400 with limited strain hardening, a simple bilinear model was used, with a yield stress of 304 MPa and strain hardening of 1.1% approximated from the tensile coupon test. The simulation agreed well with test results before fracture occurred at a drift ratio of 2%.

Design procedure

Fig. 12 shows the proposed design procedure for the SSSW. Overall dimensions of the wall (width *B* and height *H*) are determined based on architectural dimensions. The demands of yield strength Q_y and stiffness K are determined by the expected lateral load distribution and addition of stiffness for each story, respectively. Because a smaller aspect ratio of the link ($\alpha = l / b$) gives larger Q_y and K values, a relatively small α should be used. Considering the balance between the dimensions and strength desired in design, feasible values for α are 3–10. According to Eq. (3), a proper plate thickness *t* can be chosen to satisfy the required Q_y; then, according to Eq. (5), K can be met by assigning a certain value for the slit fraction ($\beta = ml / H$). β should be between 0.65 and 0.85 to ensure that individual links control the wall behavior. A suitable β can be obtained by adjusting either α or *t*, or both. After the determination of β, the number of rows of links m is decided, which gives the link length, $l = \beta H / m$, and width,

$b = l / \alpha$. By neglecting the slit width, the number of links in the direction of the wall's width is obtained as $n = B / b$. The initial design is now complete.

Next, the width-to-thickness ratio of the link (*b*/*t*) should be checked considering the sequence of nonlinear behavior. To dissipate more energy, individual links should undergo sufficient in-plane plastification prior to the local buckling of links, which can be achieved by having links with a small enough *b*/*t*. The *b*/*t* threshold that ensures in-plane behavior should be determined by the specific steel. For the LYP100 in this study, the *b*/*t* threshold is proposed to be five. If *b*/*t* is larger than the threshold after the initial design, a smaller *b*/*t* can be obtained by increasing either α, *t*, or m. Several iterations may be needed before completion of the design until *b*/*t* is below the threshold value.

Conclusions

The authors presented the design of SSSWs made from LYP100, which eliminated fracture at link ends and showed a sound energy dissipation capacity without the need for out-of-plane constraints. The major findings are summarized as follows:

(1) The feasibility of having the same strength and stiffness by adjusting link dimensions and the number of rows of links was verified experimentally. This demonstrates the flexibility of the SSSW design. The predicted yield strength and stiffness obtained using equations in previous research agree well with experimental results.

(2) For the LYP100 steel, an upper boundary width-to-thickness ratio of five ensured the in-plane behavior of individual links. By increasing the number of rows of links with the same shear strength and stiffness, a small width-to-thickness ratio of the link was realized and "fat" hysteretic loops were obtained without the need for out-of-plane constraints.

(3) The large strain hardening of LYP100 adjusted the strength of each row, resulted in evenly deformed links in multiple rows, and dissipated more energy by the sufficient development of plasticity in all links. Fracture was eliminated because of its large ductility.

(4) An SSSW design procedure was proposed, in which the aspect ratio and width-to-thickness ratio of the link and the slit fraction are considered to meet the required shear strength and stiffness while ensuring a good energy dissipation capacity.

(5) The combined hardening model in ABAQUS presented well the large strain hardening of LYP100 and can be used to estimate the maximum strength and hysteric behavior of SSSWs made from LYP100.

(6) Further work is required to make the proposed system suitable for practical applications. The threshold value *b/t* that ensures stable hysteresis must be quantified. The design yield strength of LYP, which is characterized by conspicuous strain hardening, must be determined. Such strength is needed to estimate the energy dissipation of the slitted wall and the design of the surrounding frame to ensure that it can sustain the strength transferred from the wall.

References

American Institute of Steel Construction (AISC) (2010). "Seismic Provisions for Structural Steel Buildings." *ANSI/AISC 341-10*, Chicago.

Berman J. and Bruneau M. (2005). "Experimental investigation of light-gauge steel plate shear walls." *J. Struct. Eng.*, 10.1061/(ASCE)0733-9445(2005)131:2(259), 259-267.

Canadian Standard Association (CSA) (2009). "Design of steel structures." *CSA S16-09*, Mississauga, ON, Canada.

Chen S. and Jhang C. (2006). "Cyclic behavior of low-yield point steel shear walls." *Thin-Walled Structures*, 44(7), 730-738.

Chopra A. K. (2000). *Dynamics of Structures: Theory and Applications to Earthquake Engineering* (2nd edition). Prentice Hall: New Jersey, USA.

Cortes G. and Liu J. (2011). “Experimental evaluation of steel slit panel frames for seismic resistance.” *Journal of constructional steel research*, 67(2), 181-191.

Dassault Systèmes (2004). “ABAQUS Ver. 6.10 User’s Manual.” (http://www.abaqus.com)

Hitaka T., Ito M., Murata Y., and Nakashima M. (2009). “Seismic behavior of steel shear plates stiffened by wood panels.” *Proc., Behavior of Steel Structures in Seismic Areas (STESSA)*, Philadelphia, PA, 623-628.

Hitaka T. and Matsui C. (2003). “Experimental study on steel shear wall with slits.” *J. Struct. Eng.*, 10.1061/(ASCE)0733-9445(2003)129:5(586), 586-595.

Hitaka T., Matsui C. and Sakai J. (2007). “Cyclic tests on steel and concrete-filled tube frames with slit walls.” *Earthquake Engng Struc. Dyn.*, 36(6), 707-727.

Ke K. and Chen Y.Y. (2012). “Design method of steel plate shear wall with slits considering energy dissipation.” *Proc., 15th World Conference on Earthquake Engineering*, Lisboa, Portugal.

Ma X, Borchers E, Peña A, Krawinkler H, Billington S, Deierlein G. (2010). “Design and behavior of steel shear plates with openings as energy-dissipating fuses.” John A. Blume Earthquake Engineering Center Technical Report 173, Stanford Digital Repository.

Martinez-Rueda J. E. (2002). “On the evolution of energy dissipation devices for seismic design.” *Earthquake Spectra*, 18(2), 309-346.

Matteis G., Landolfo R. and Mazzolani F. (2003). “Seismic response of MR steel frames with low-yield steel shear panels.” *Engineering Structures*, 25(2), 155-168.

McCloskey DM. (2006). "Steel slit panels for lateral resistance of steel frame buildings." M.S. thesis, West Lafayette (Indiana), Purdue University.

Nakashima M. (1995). "Strain-hardening behavior of shear panels made of low-yield steel. I: test." *J. Struct. Eng.*, 10.1061/(ASCE)0733-9445(1995)121:12(1742), 1742-1749.

Nakashima M., Akazawa T., Tsuji B. (1995). "Strain-hardening behaviour of shear panels made of low yield steel, II: Model." *J. Struct. Eng.*, 10.1061/(ASCE)0733-9445(1995)121:12(1750), 1750-1757.

Qu B, Bruneau M, Lin CH, Tsai KC (2008). "Testing of full-scale two-story steel plate shear wall with reduced beam section connections and composite floors." *J. Struct. Eng.*, 10.1061/(ASCE)0733-9445(2008)134:3(364), 364-373.

Roberts T. M. and Ghomi S. Sabouri (1991). "Hysteretic characteristics of unstiffened plate shear panels." *Thin-Walled Struct.*, 12(2), 145-162.

Timoshenko S.P. and Gere J.M. (1961). *Theory of Elastic Stability* (2nd edition). McGraw-Hill: New York.

Vian D. (2005). "Steel plate shear walls for seismic design and retrofit of building structures." Ph.D. dissertation, SUNY at Buffalo: Buffalo, New York.

Zhang C., Zhang Z. and Shi J. (2012). "Development of high deformation capacity low yield strength steel shear panel damper." *Journal of Constructional Steel Research*, 75, 116-130.

List of tables

List of figures

Table 1. Summary of specimens

Specimen	Material	t (mm)	b (mm)	l (mm)	m	α	β	b/t	Q_y (kN)	K (kN/mm)	Q_y / K (%)
1	LYP100	9	70.3	410	2	5.8	0.71	7.8	90.3	69.6	0.11
2	LYP100	9	45.5	267	3	5.9	0.70	5.1	89.3	70.3	0.11
3	LYP100	9	22.5	133	6	5.9	0.69	2.5	87.7	69.0	0.11
4	SS400	4.2	32.4	243	2	7.5	0.42	7.7	103.0	36.0	0.25

Table 2. Strength and stiffness

Specimen	$Q_{y.t}$ / Q_y	$Q_{1\%.t}$ (kN)	Q_p (kN)	$Q_{\max.t}$ / Q_p	K_t (kN/mm)	K_t / K
1	0.99	181.2	135.4	2.09	68.5	0.98
2	1.04	182.9	134.0	2.38	69.9	1.00
3	1.16	187.5	131.5	2.24	68.2	0.99
4	1.06	180.6	154.4	1.25	35.8	0.99

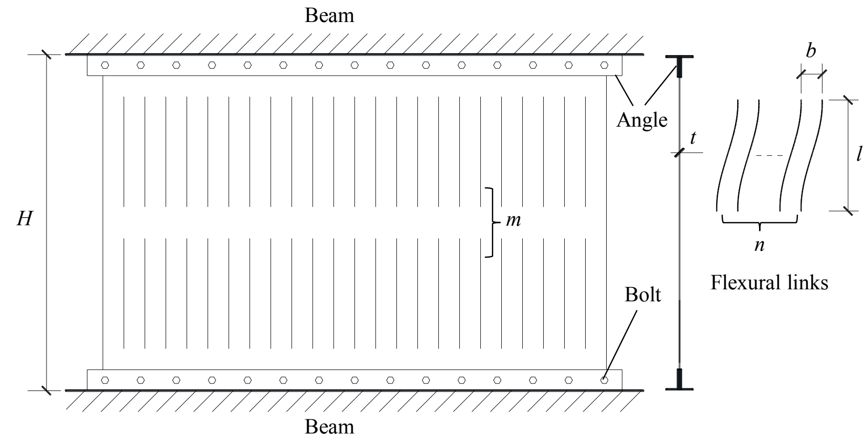

Fig. 1. Steel slit shear wall

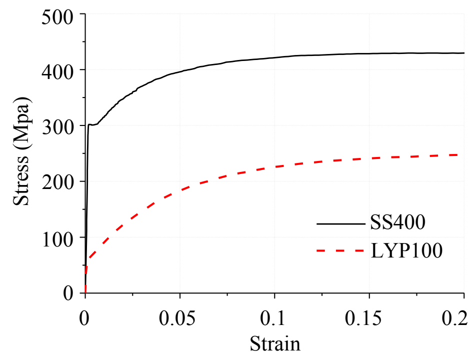

Fig. 2. Stress-strain relationship of LYP100

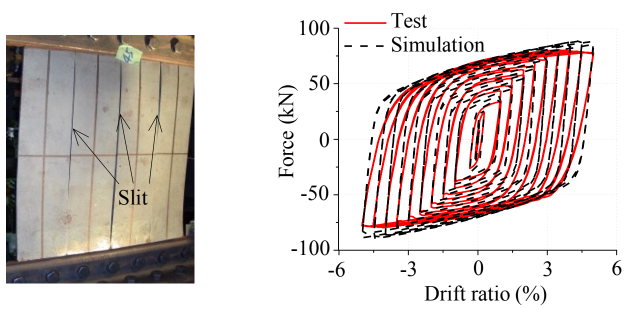

(a) (b)

Fig. 3. A slit shear wall tested: (a) test specimen; (b) hysteretic curves

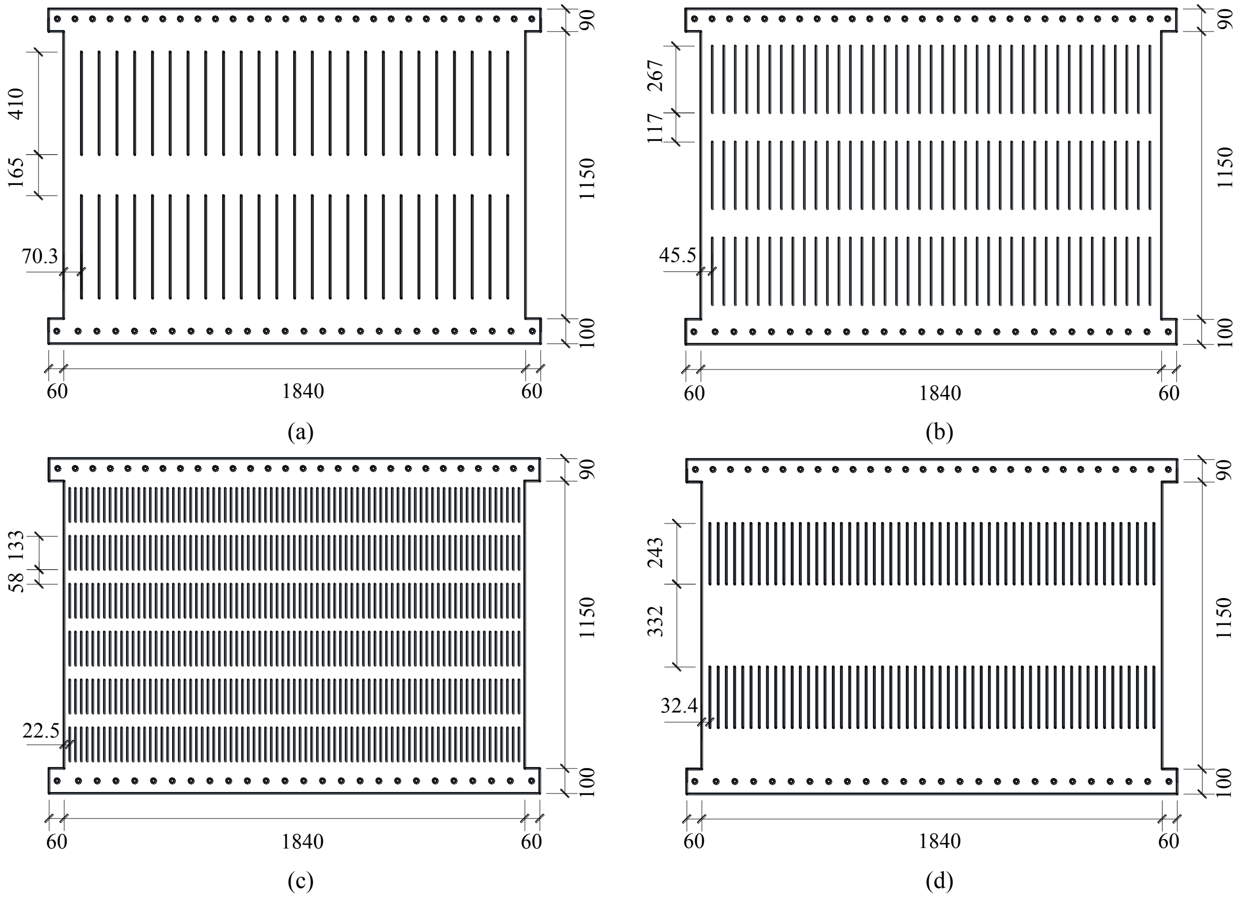

Fig. 4. Details of specimens (unit: mm): (a)–(d) Specimens 1–4

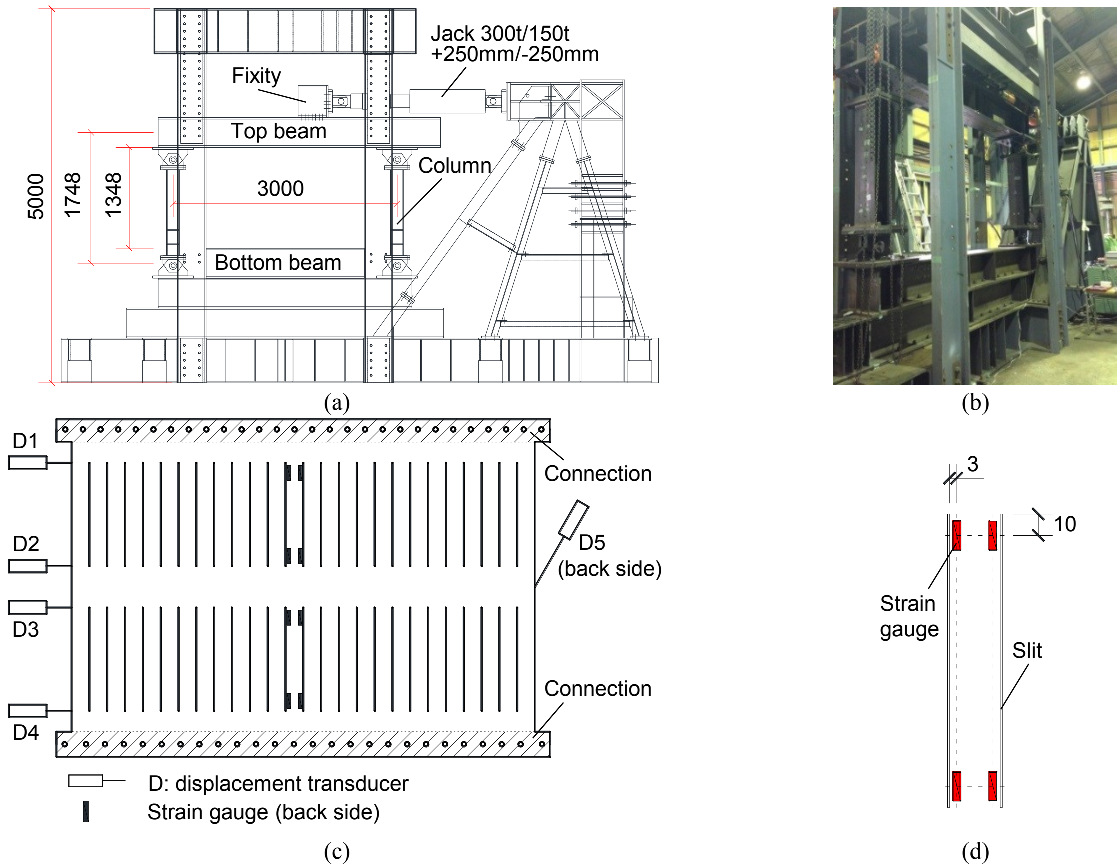

Fig. 5. Setup and instrumentation: (a) loading frame; (b) test setup; (c) placements of displacement transducers and strain gauges (Specimen 1 for reference); (d) strain gauges in detail

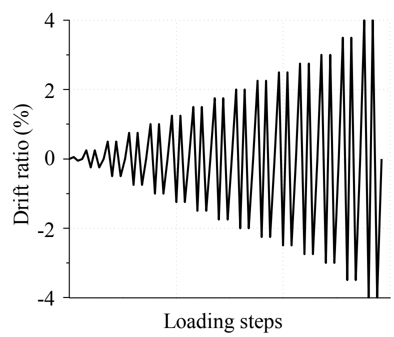

Fig. 6. Incremental two-cycle loading

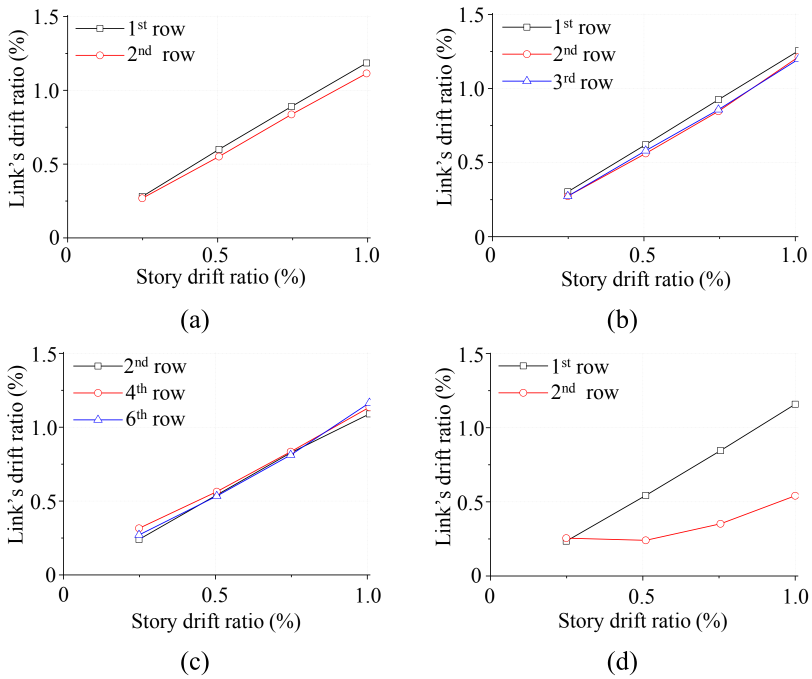

Fig. 7. Distribution of shear deformation among rows: (a)–(d) Specimens 1–4

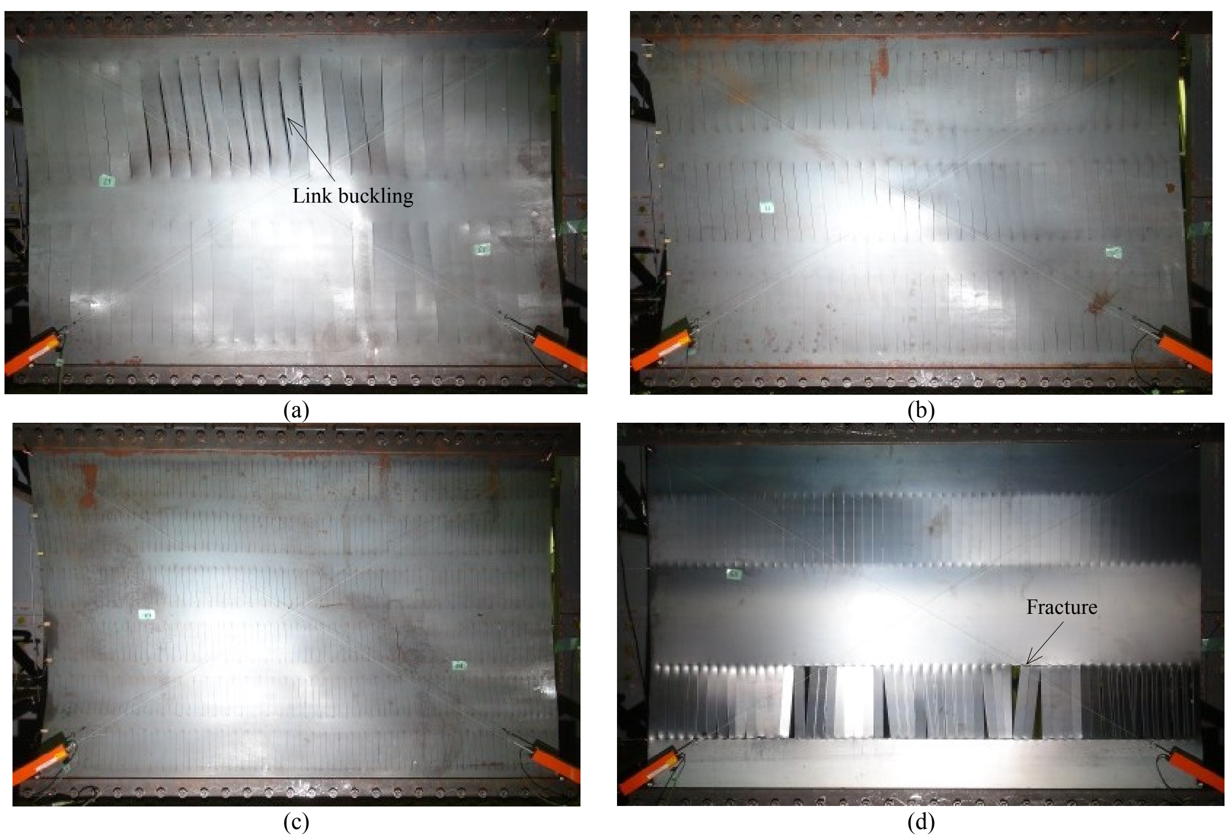

Fig. 8. Link buckling and fracture: (a)–(d) Specimens 1–4

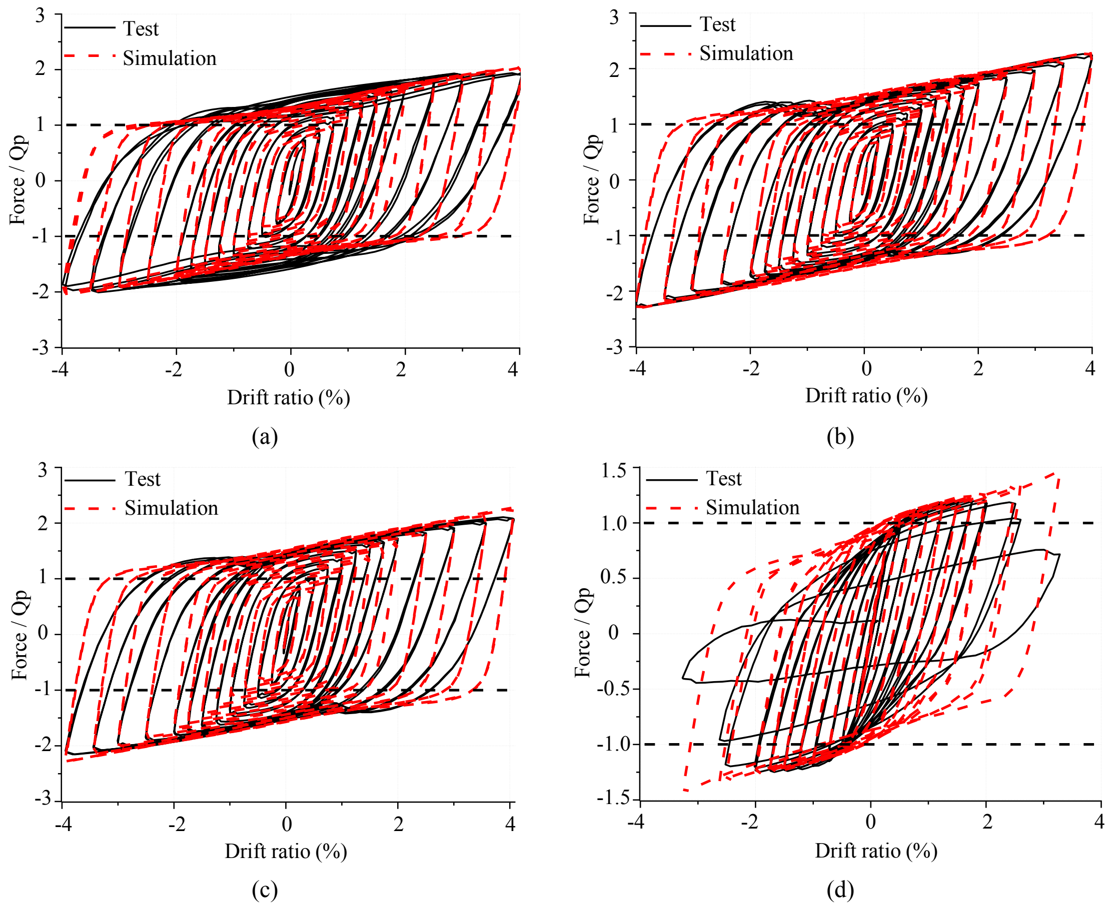

Fig. 9. Hysteretic curves: (a)–(d) Specimens 1–4

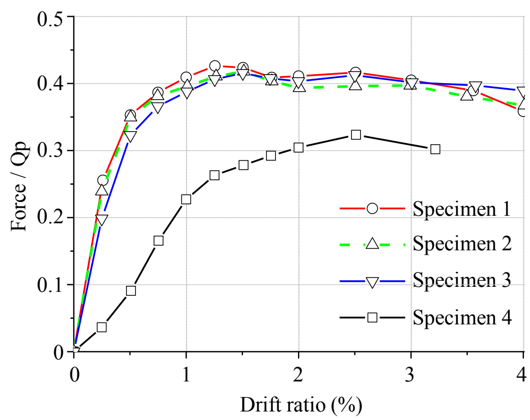

Fig. 10. Equivalent damping ratios

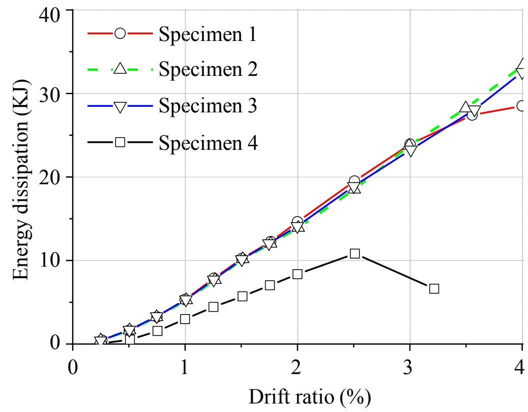

Fig. 11. Energy dissipation

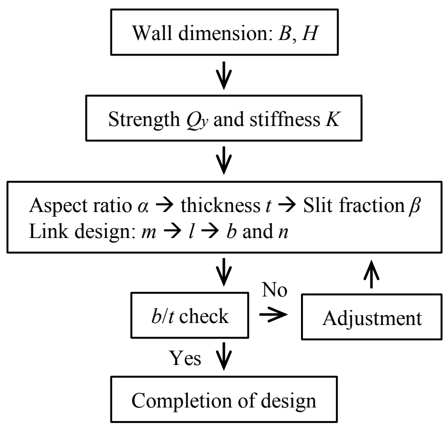

Fig. 12. Flow chart of design procedure